2017 IEEE/RSJ International Conference on Intelligent Robots and Systems (IROS)
September 24–28, 2017, Vancouver, BC, Canada

A Five Degree-of-Freedom Body-Machine Interface for Children with Severe Motor Impairments

Sheryl Chau[1], Sanders Aspelund[1], Ranjan Mukherjee[1],
Mei-Hua Lee[2], Rajiv Ranganathan[1,2], and Florian Kagerer[2]

Abstract— **Children with severe motor impairments require the use of assistive devices to perform activities of daily living. Brain-machine interfaces are not suited for children due to various factors such as surgical risks. In this paper, we present a non-invasive body-machine interface where upper body movements are recorded by wireless inertial measurement units (IMUs) and used to control a robot arm. We develop a novel approach, called the virtual body model (VBM), which allows for control of high number of degrees-of-freedom (DOF). Our results show that participants could use the VBM to control up to five DOFs of a robot arm, and perform a pick-and-place task. Even with minimal training, trajectories of the end effector were smooth and positioning was accurate. These results show the potential of this safe, non-invasive approach to control high DOFs in children.**

NOMENCLATURE

BMI : Brain Machine Interface
BoMI : Body Machine Interface
DOF : Degree of Freedom
PCA : Principal Components Analysis
VBM : Virtual Body Model

I. INTRODUCTION

The 2010 American Census estimates that approximately 2,000,000 children under 15 years of age have a disability of some kind, and that 15% of these children need some form of assistance when performing activities for daily living [1]. Assistive devices for movement and mobility are a critical need for these children since they not only facilitate sensorimotor development but promote psychosocial development by enabling interaction with peers.

One critical challenge in the use of assistive devices is that there is a tremendous diversity in the types of devices (e.g., wheelchair, robot arm, computer) and children have to learn to control these devices using many different interfaces (e.g., joysticks, head arrays, specialized mouse). In view of this challenge, there has been a push for designing a general-purpose human-machine interface that can be used to 'control' a variety of assistive devices. This is especially critical for children with severe motor impairments who may be limited in their ability to use device-specific interfaces.

There are two types of general-purpose interfaces that are commonly used: Brain-Machine Interface (BMI) and Body-Machine Interface (BoMI). BMIs [2]–[7] require sensors to be implanted internally or applied externally to obtain brain signals and have many disadvantages for their use by children. First, BMIs do not take advantage of the body's movement repertoire; this makes them suitable mainly for conditions where there is almost a complete loss of movement, which is atypical in children. Second, invasive BMIs, where electrodes are physically implanted in the brain, involve risks of surgery, a potential for infection, and a limited life of electrodes. This makes the technology unsustainable for use in children who have several decades of life ahead of them. To our knowledge, only one study has tested an invasive BMI and this was done in children with epilepsy who already needed surgery [8]. Finally, non-invasive BMIs such as Electroencephalogram (EEG), where brain signals are measured from the scalp, have low signal-to-noise ratios, making them slow to operate. There has been some work in children where EEG has been used to drive a video game [9], but none on movement control. From a daily user's perspective, current EEG technology is cumbersome (a typical 64-channel EEG requires at least 20-30 minutes of preparation, using gel to get good, reliable signals). Dry electrode EEG setups (which circumvent some of these challenges) have been improving rapidly and are easier to use, but are not comfortable for prolonged use in children for daily activities.

BoMIs refer to interfaces that rely on movements of the user. For users with severe motor impairments, BoMIs have been designed to capture movements of the upper body using inertial measurement units (IMUs). Such BoMIs are better suited for children since they are non-invasive, robust, and do not disrupt natural communication while the interface is being used. The feasibility of BoMIs have been demonstrated in adults with spinal cord injury in low degree-of-freedom (DOF) tasks [10], [11] and for assistive devices [12], [13] but there are significant theoretical and practical challenges that have to be addressed before BoMIs can be successfully used by children, and used for high-DOF tasks. To overcome these challenges, some of which will be discussed in Section II, a new BoMI will be introduced in this paper. This BoMI, which will enable children without limbs control an assistive device, uses a Virtual Body Model (VBM) to map and project the upper body movements of the user onto a pre-defined set of anatomically distinct motion patterns. These projections can be used to control the individual DOFs of an assistive device, such as a robot manipulator. Section III describes the VBM and a set of anatomically distinct motion patterns of the human upper body. Section

[1] Department of Mechanical Engineering, Michigan State University, East Lansing, MI 48824, USA
[2] Department of Kinesiology, Michigan State University, East Lansing, MI 48824, USA

IV describes the algorithm used to map and project the user movements onto the anatomically distinct motion patterns. Section V describes the experimental hardware and presents preliminary experimental results. Concluding remarks are provided in Section VI.

II. Limitations of Current BoMIs

BoMIs currently use the Principal Component Analysis (PCA) approach to processing sensor signals. PCA has been widely used as a dimensionality reduction technique to describe how the nervous system coordinates a large number of DOFs in the human body [14], [15]. In studies of hand and finger coordinations that examined how people grasp a large number of everyday objects (e.g., apple, comb, frying pan, toothpick, etc), it was found that the first two principal components were sufficient to account for 80-85% of the variance in the data [14]. These results have been used as evidence to support that the nervous system simplifies control of a large number of DOFs by linking them into a smaller number of 'movement primitives' or 'synergies' [16], [17].

Although PCA works well in describing the coordination between high DOFs, there are two limitations when it is used for control of a high-DOF task. First, PCA yields principal components in descending order of their variance (eigenvalues). This means that while the first couple of DOFs are easy to control, additional DOFs, which are associated with higher principal components, are difficult to control. Second, PCA looks for directions of maximum variance, and enforces components to be mutually orthogonal. This can become disadvantageous from a control standpoint because: (i) the components can be linear combinations of motions at several joints, making it harder to control motions along these directions independently; (ii) the components become 'less intuitive' since they may not correspond to distinct anatomical motions. For example, when using PCA to control a 3-DOF task, learning was significantly longer (2-4 times longer) compared to 1 or 2-DOF tasks [18]. These limitations motivate the development of an 'intuitive' BoMI that can be used to control a multi-DOF robot arm and its grasper. Fall et al. [19] developed an intuitive BOMI using the head as a virtual joystick; the virtual joystick was used to control three-DOFs and shoulder movements were used to toggle between multiple sets of DOFs. The BoMI developed in this paper relies on the VBM (discussed in the next section) to create an unambiguous 'body language' that can be used to control the robot DOFs and perform a meaningful task.

III. The VBM and a Set of Anatomically Distinct Motion Patterns

A. The Finite Element VBM

The VBM is a finite element model of the upper body of the human user, comprised of the head, neck and torso. Since our objective has been to enable a user without limbs to control an assistive device, the arms were not included in the model. The VBM models the upper body without using articulated joints, relying completely on deformation due to the application of external forces. Figure 1 shows

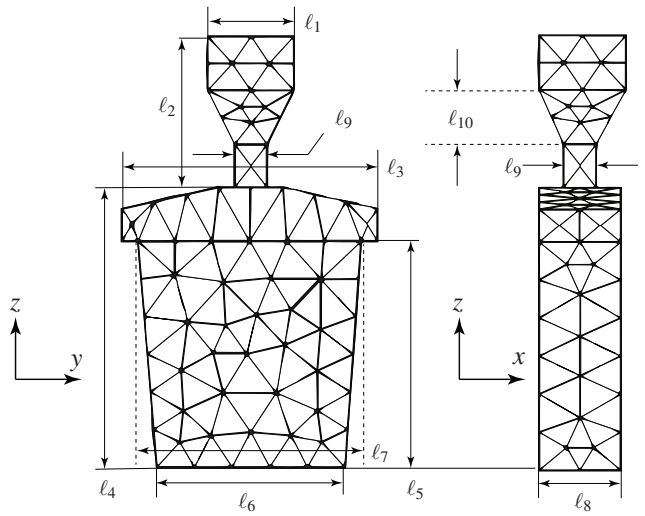

Fig. 1. VBM dimensions: head width ℓ_1, distance from top of the head to base of the neck ℓ_2, shoulder span ℓ_3, torso height ℓ_4, length from under arm to waist ℓ_5, width of waist ℓ_6, chest span ℓ_7, torso thickness ℓ_8, neck thickness and width ℓ_9, and height of the lower portion of the head ℓ_{10}.

an example VBM, defined by the dimensional parameters ℓ_i, $i = 1,2,\cdots 10$. These parameters will be chosen based on measurements of the upper body dimensions of the user. For the sake of simplicity, the VBM was assumed to be isotropic, but more accurate models may vary the material property to reflect different levels of mobility of different parts of the upper body of the user. To obtain a 3D mesh, the VBM was created with the commercial software ANSYS using tetrahedral elements. The number of elements were automatically chosen by the software, and the nodes, comprised of the vertices of all the tetrahedral elements, were assumed to have three DOFs in the inertial xyz Cartesian coordinate system. Assuming the total number of nodes to be n, the displacements of the i-th node to be (u_{xi}, u_{yi}, u_{zi}), and the external forces acting on the i-th node along the x, y, z directions to be (f_{xi}, f_{yi}, f_{zi}), the linear elastic relationship between the forces and displacements can be expressed as follows

$$F = KU \tag{1}$$

where

$$F \triangleq \begin{bmatrix} f_{x1} & f_{y1} & f_{z1} & \cdots & f_{xn} & f_{yn} & f_{zn} \end{bmatrix}^T$$
$$U \triangleq \begin{bmatrix} u_{x1} & u_{y1} & u_{z1} & \cdots & u_{xn} & u_{yn} & u_{zn} \end{bmatrix}^T$$

and K is the $3n \times 3n$ stiffness matrix, which can be obtained using standard finite element methods. Since the VBM aims to replicate the movement of the human user, we rewrite Eq.(1) as

$$U = CF, \qquad C \triangleq K^{-1} \tag{2}$$

where C is the compliance matrix and can be computed from K off-line.

B. A Set of Five Anatomically Distinct Motion Patterns and Associated Forces

In this section we define a set of five anatomically distinct motion patterns of the human upper body that can be used to control four DOFs of a robot end-effector and one DOF of the grasper in the end-effector. The anatomically distinct motion patterns should be selected such that the mapping between the upper body movements of the user and the movements of the end-effector in the inertial coordinate system is intuitive. Furthermore, the user should be able to produce these motion patterns repeatedly, independently as well as simultaneously, and with relative ease. The five distinct motion patterns that were selected are described below with the help of the VBM in Fig.2:

1) Torso flexion and extension - This motion can be produced in the VBM by applying the single force P_1, as shown in Fig.2 (b). Since the virtual body bends forward in the x direction by angle α, this motion will be mapped to the translational movement of the end-effector in the x direction.
2) Torso lateral flexion - This motion can be produced in the VBM by applying the single force P_2, as shown in Fig.2 (c). Since the virtual body bends laterally in the y direction by angle β, this motion will be mapped to the translational movement of the end-effector in the y direction.
3) Torso rotation - This motion can be produced in the VBM by applying the couple shown in Fig.2 (d). Since the virtual body rotates about the z axis by angle γ, this motion will be mapped to the translational movement of the end-effector in the z direction following the notion of screw theory.
4) Neck lateral flexion - This motion can be produced in the VBM by applying the couple shown in Fig.2 (e). Since the head rotates about the x axis by angle δ, this motion will be mapped to the rotational movement of the end-effector about the x axis.
5) Scapular protraction and retraction - This motion can be produced by the set of three equilibriating forces shown in Fig.2 (e). This motion of the virtual body will be mapped to opening and closing motion of the grasper.

It is clear from the above discussion that although the vector F in Eq.(2) has dimension $3n$, all but 9 entries will have zero values. This is true because P_1 and P_2 are both applied at a single node on the VBM, P_3 and P_4 are both applied at 2 nodes, and forces proportional to P_5 are applied at 3 nodes.

C. Virtual Sensors on the VBM

We assume that there are k virtual sensors placed on the VBM, where k is the number of IMUs placed on the upper body of the user. The locations of the virtual sensors are chosen to closely match those of the IMUs. The VBM is comprised of tetrahedral elements and each virtual sensor is placed on the triangular face of a tetrahedral element that lies on the surface of the VBM - see Fig.3. The deformation of the VBM will be captured by the virtual sensors; for each sensor, this deformation can be quantified by the displacements of the three nodes of the triangular face on which the sensor is affixed. Since there are k sensors, each sensor is associated with 3 nodes, and each node has 3 displacements, we are interested in $9k$ elements of the U vector in Eq.(2); let $\bar{U}$ define this vector. It is clear from this discussion and the discussion in the last section that Eq.(2) can be truncated to a form where the C matrix is of dimension

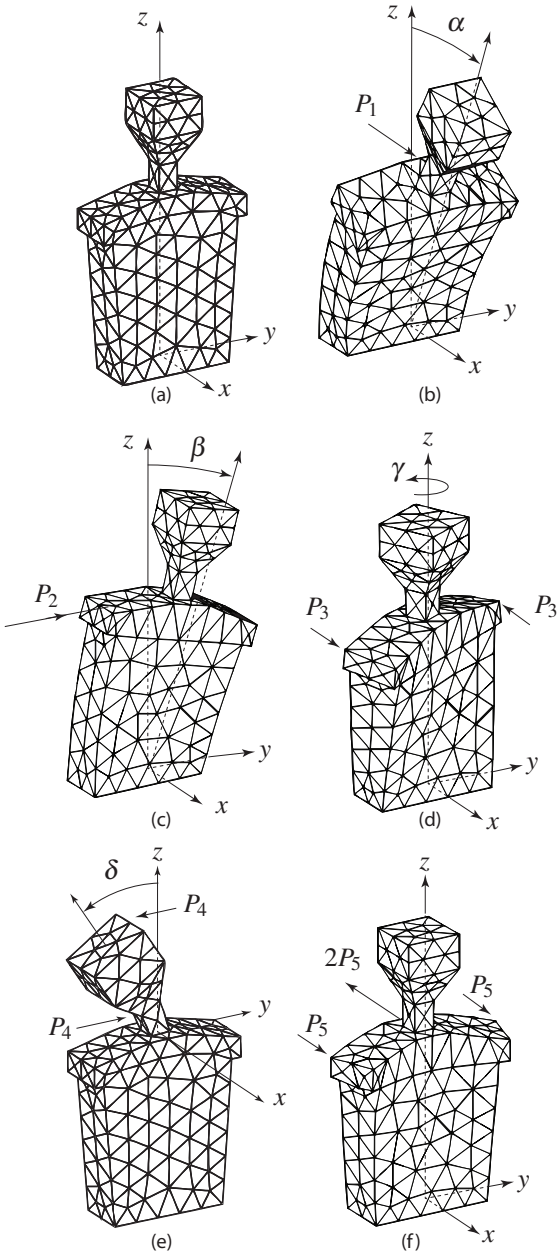

Fig. 2. (a) Undeformed configuration of the VBM, (b), (c), (d), and (e) show five deformed configurations of the VBM corresponding to five anatomically distinct motion patterns of the upper body. The five anatomically distinct motion patterns are: (b) torso flexion and extension, (c) torso lateral flexion, (d) torso rotation, (e) neck lateral flexion, and (f) scapular protraction and retraction.

$9k \times 9$. Among the 9 entries of F, only five are independent; therefore, Eq.(2) can be further simplified to the form

$$\bar{U} = \bar{C}P, \qquad P \triangleq \begin{bmatrix} P_1 & P_2 & P_3 & P_4 & P_5 \end{bmatrix}^T \tag{3}$$

where $\bar{C}$ is a matrix of dimension $9k \times 5$.

IV. Projecting User Movements Onto Anatomically Distinct Motion Patterns

To project the user movements onto anatomically distinct motion patterns, we adopt the following two-step procedure:

1) We will use the measurements from the IMUs to determine how the VBM should deform such that it replicates the movement of the user.
2) We will compute the forces P_i, $i = 1,2,\cdots,5$, such that the error between the deformation of the VBM due to application of the forces and the desired deformation, obtained from step 1, is minimized.

Each force P_i, $i = 1,2,\cdots,5$, obtained in step 2 can be viewed as a projection of the movement of the user onto the different anatomically distinct motion patterns, defined earlier. This is true because each one of these anatomically distinct motion patterns can only be generated by one of these forces.

To replicate the movement of the user by the VBM in step 1, we note that the upper body movements of the user will be sensed by the set of k IMUs. Each IMU is tared after placement and provides the data for computation of the rotation matrix R that maps a vector from the undeformed configuration to the deformed configuration. We use this information to determine the desired orientation of unit vectors in the local neighborhood of each virtual sensor. If a_j, b_j, and c_j denote the three specific nodes of the VBM associated with the j-th virtual sensor, $\zeta_{j,\text{orig}}$ and $\eta_{j,\text{orig}}$ define the unit vectors in the initial undeformed configuration (see Fig.3), and R_j denotes the rotation matrix obtained from the j-th IMU, the desired unit vectors $\zeta_{j,\text{des}}$ and $\eta_{j,\text{des}}$ can be obtained using the relations

$$\zeta_{j,\text{des}} = R_j\,\zeta_{j,\text{orig}}, \quad \eta_{j,\text{des}} = R_j\,\eta_{j,\text{orig}}, \qquad j = 1,2,\cdots,k \tag{4}$$

To determine the forces P in step 2, we start with the initial guess $P = 0$. Equation (3) indicates that there exists an implicit functional description of the unit vectors as follows

$$Y = g(P), \qquad Y \triangleq \begin{bmatrix} \zeta_1 & \eta_1 & \cdots & \cdots & \zeta_k & \eta_k \end{bmatrix}^T$$

The Jacobian of the vector function is computed numerically and the Newton-Raphson method is used along with the method of least-squares [20] to estimate P as follows

$$P = (J^T J)^{-1} J^T (Y_{\text{des}} - Y_{\text{orig}}), \qquad J \triangleq \left[\frac{\partial g}{\partial P}\right] \tag{5}$$

In the above equation, J is the Jacobian matrix and Y_{des} and Y_{orig} are defined as

$$Y_{\text{des}} \triangleq \begin{bmatrix} \zeta_{1,\text{des}} & \eta_{1,\text{des}} & \cdots & \cdots & \zeta_{k,\text{des}} & \eta_{k,\text{des}} \end{bmatrix}^T$$
$$Y_{\text{orig}} \triangleq \begin{bmatrix} \zeta_{1,\text{orig}} & \eta_{1,\text{orig}} & \cdots & \cdots & \zeta_{k,\text{orig}} & \eta_{k,\text{orig}} \end{bmatrix}^T$$

The forces P obtained from Eq.(5) are the projections of the movement of the user onto the different anatomically distinct motion patterns, as discussed earlier in this section.

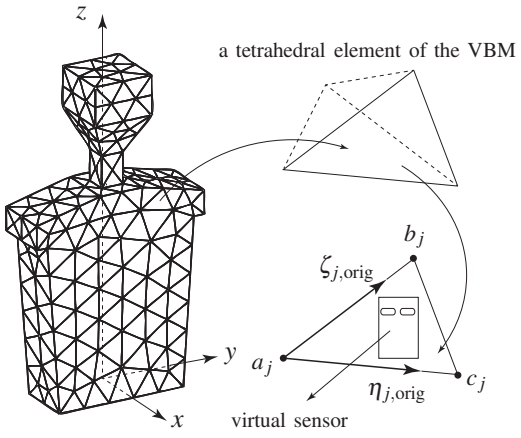

Fig. 3. Placement of the j-th virtual sensor, $j \in \{1,2,\cdots,k\}$, on the triangular face of a tetrahedral element of the VBM. The nodes of the triangular element are marked as a_j, b_j and c_j; a_j is arbitrarily selected as the base node and $\zeta_{j,\text{orig}}$ and $\eta_{j,\text{orig}}$ are unit vectors from the base node to the other two nodes in the initial undeformed configuration.

V. Experimental Validation

A. Experimental Hardware

The experimental hardware is comprised of the Kinova JACO 3 Fingers robot arm (see Fig.4) and a set of $k = 5$ wireless IMUs manufactured by YOST Labs. The robot arm has 7 DOFs including the grasper DOF. In our experiments, 5 DOFs were used: these include three-dimensional translation in the Cartesian space of the end-effector, wrist rotation, and opening and closing of the grasper. The IMUs (35 mm $\times$ 60 mm $\times$ 15 mm) were mounted on a vest and a cap worn by the user (see Fig.5); an adult without impairment was chosen as the user for experimental verification of the BoMI.

Fig. 4. The Kinova JACO 3 Finger robot.

B. VBM of the User

The adult user was a college-aged male with no impairment. Based on the measurements of his upper body, the VBM dimensions were chosen as follows

$$\ell_1 = 16.0 \quad \ell_2 = 32.0 \quad \ell_3 = 47.5 \quad \ell_4 = 52.0 \quad \ell_5 = 42.0$$
$$\ell_6 = 35.0 \quad \ell_7 = 41.5 \quad \ell_8 = 16.0 \quad \ell_9 = 6.0 \quad \ell_{10} = 12.0$$

where the units are centimeters. A 3D mesh of the VBM was generated using tetrahedral elements in ANSYS; it resulted in 883 elements and $n = 283$ nodes. The Young's modulus and Poisson's ratio of the VBM were chosen as

$$E = 4000\,\text{MPa} \qquad \nu = 0.33$$

Five virtual sensors were placed on the VBM at locations that closely matched those of the 5 IMUs on the user. The number and location of the IMUs placed on the user were determined through trial and error.

Fig. 5. Five IMUs attached to the cap and vest of the user are circled in the (a) front and (b) back views of the user: three are located on the vest and the other two are placed on the top and back of the cap.

C. Robot Control with User-in-the-Loop

A block diagram of the robot control system with user-in-the loop is shown in Fig.6. The user picks a target location for the robot end-effector and determines the error relative to the current location. To eliminate the error, the user moves the upper body using the pre-defined anatomically distinct motion patterns proportional to the error. The VBM replicates the movement of the user based on measurements obtained from the IMU sensors. The VBM outputs the forces P_i, $i = 1, 2, \cdots, 5$, which are the estimates of the anatomically distinct motion patterns generated by the user. These forces are mapped to desired velocities of the end-effector which are tracked by the internal controller of the robot.

D. Experimental Results

The BoMI was used to control the Kinova robot arm to pick and place a plastic water bottle. Starting from its initial position, the end-effector was required to reach the first target location, where the water bottle is located. The

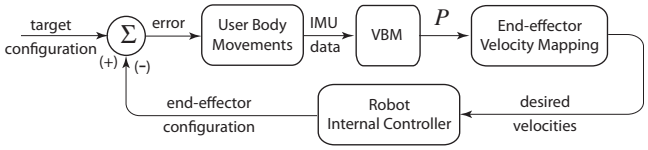

Fig. 6. Block diagram of robot control system with user-in-the loop.

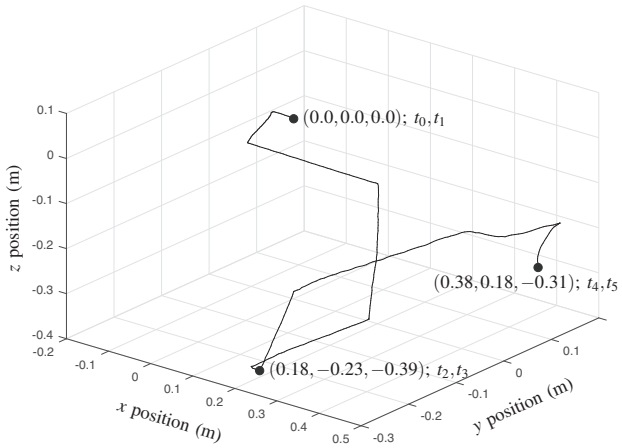

Fig. 7. End-effector trajectory in Cartesian coordinates during user trial.

end-effector was then required to grasp the bottle, pick it up, and deliver it to the second target location. The user, seated approximately 50 cms from the base of the robot and facing in the positive x direction, was given several practice runs before the actual trial. The total time for practice was approximately 30 minutes. Figure 7 shows the trajectory of the end-effector and Fig.8 shows the x, y, z positions of the end-effector, wrist rotation angle, and grasper configuration as a function of time. The results of the user trial is described below with the help of Figs.7 and Fig.8:

- From $t_0 = 0.0$ s to $t_1 = 7.0$ s, the BoMI was used to rotate the wrist to achieve "ready-to-grasp" configuration - see Fig.8. During this time period, the end-effector

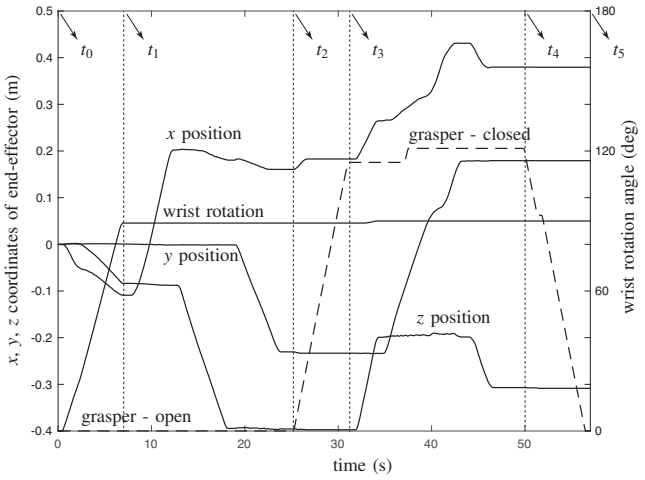

Fig. 8. Variation of Cartesian coordinates of the end-effector, wrist rotation, and grasper configuration with time for the user trial.

position did not change significantly.

- From $t_1 = 7.0$ s to $t_2 = 25.2$ s, the BoMI was used to move the end-effector to the location of the water bottle along the trajectory shown in Fig.7. It can been seen from Fig.8 that x, y, z positions of the end-effector changed during this time period.
- From $t_2 = 25.2$ s to $t_3 = 31.1$ s, the BoMI was used to grasp the water bottle; the grasper was originally in its open configuration - see Fig.8.
- From $t_3 = 31.1$ s to $t_4 = 50.0$ s, the BoMI was used to move the water bottle to its desired location; during this time, the grasper remained closed.
- From $t_4 = 50.0$ s to $t_5 = 56.6$ s, the BoMI was used to release the water bottle.

The entire task took the user 56.6 s to complete. The smooth trajectory in Fig.7 suggests that the user was able to approach the target configurations without having to make adjustments. Since the user had the opportunity to practice only a few times before the trial, we expect the time required for the task to decrease with more practice. In this regard, it should be mentioned that limits were placed on the maximum velocity of the robot for safety.

As supplemental material, we have uploaded a video clip of the user trial.

VI. Conclusion

A new Body-Machine Interface (BoMI) was presented in this paper. It relies on the construction of the Virtual Body Model (VBM), which is a finite element model of the upper body of the user, for transformation of body-mounted sensor signals into pre-defined, anatomically distinct motions. These anatomically distinct motions can be generated both independently and simultaneously. By mapping them to the individual degrees-of-freedom (DOF) of an assistive device, such as robot arm, the BoMI can be used to control the device and perform a meaningful task using upper body movements. Compared to Principal Components Analysis (PCA) based methods that have been used in prior BoMIs, the VBM method allows for control of higher number of DOFs and makes the BoMI intuitive to use. This ability to provide intuitive control may be especially important for learning in children as it reduces the computational burden. For experimental validation of the BoMI, a college-aged male was recruited to perform a pick-and-place task involving five DOFs using a robot arm. The experimental results show that the user, after a few practice runs, was able to perform the task with relative ease. The time required for performing the task was also reasonable considering the fact that limits were placed on the maximum velocity of the robot to ensure safety. Future studies will focus on developing the interface further for tasks requiring higher DOFs and examine the ability of children to learn to use the interface quickly.

Acknowledgements

The authors gratefully acknowledge the financial support provided by the office of the Vice President for Research and Graduate Studies at Michigan State University and the National Science Foundation, Grant CBET-1703735.

References

[1] Brault MW. Americans with disabilities: 2010. US Department of Commerce, Economics and Statistics Administration, US Census Bureau, 2012.

[2] Donoghue JP. Connecting cortex to machines: recent advances in brain interfaces. Nature Neuroscience, 5, pp.1085-1088, 2002.

[3] Wolpaw JR, Birbaumer N, McFarland DJ, Pfurtscheller G, Vaughan TM. Brain-computer interfaces for communication and control. Clinical Neurophysiology 113.6: pp.767-791, 2002.

[4] Carmena JM, Lebedev MA, Crist RE, O'Doherty JE, Santucci DM, Dimitrov DF, Patil PG, Henriquez CS, Nicolelis MAL. Learning to control a brain-machine interface for reaching and grasping by primates. PLoS Biol 1.2: e42, 2003.

[5] Velliste M, Perel S, Spalding MC, Whitford AS, Schwartz AB. Cortical control of a prosthetic arm for self-feeding. Nature 453: 10981101, 2008.

[6] Hochberg LR, Bacher D, Jarosiewicz B, Masse NY, Simeral JD, Vogel J, Haddadin S, Liu J, Cash SS, van der Smagt P, Donoghue JP. Reach and grasp by people with tetraplegia using a neurally controlled robotic arm. Nature 485: 372-375, 2012.

[7] Bensmaia SJ, Miller LE. Restoring sensorimotor function through intracortical interfaces: progress and looming challenges. Nature Reviews Neuroscience 15.5: pp.313-325, 2014.

[8] Breshears JD, Gaona CM, Roland JL, Sharma M, Anderson NR, Bundy DT, Freudenburg ZV, Smyth MD, Zempel J, Limbrick DD, Smart WD, Leuthardt EC. Decoding motor signals from the pediatric cortex: implications for brain-computer interfaces in children. Pediatrics 128.1: e160-168, 2011.

[9] Lim CG, Lee TS, Guan C, Fung DSS, Zhao Y, Teng SSW, Zhang H, Krishnan KRR. A braincomputer interface based attention training program for treating attention deficit hyperactivity disorder. PLoS One 7.10: e46692, 2012.

[10] Casadio M, Pressman A, Fishbach A, Danziger Z, Acosta S, Chen D, Tseng H-Y, Mussa-Ivaldi FA. Functional reorganization of upper-body movement after spinal cord injury. Experimental Brain Research 207.3-4: pp.233-247, 2010.

[11] Pierella C, Abdollahi F, Farshchiansadegh A, Pedersen J, Thorp EB, Mussa-Ivaldi FA, Casadio M. Remapping residual coordination for controlling assistive devices and recovering motor functions. Neuropsychologia, 79: pp.364-376, 2015.

[12] Moreno, J. C., de Lima, E. R., Ruiz, A. F., Brunetti, F. J., Pons, J. L. Design and implementation of an inertial measurement unit for control of artificial limbs: Application on leg orthoses. Sensors and Actuators B: Chemical, 118: pp.333-337, 2006.

[13] Mandel, C., Rofer, T., Frese, U. Applying a 3DOF Orientation Tracker as a Human-Robot Interface for Autonomous Wheelchairs. Proc. IEEE 10th International Conference on Rehabilitation Robotics, pp.52-59, 2007.

[14] Santello M, Flanders M, Soechting JF. Postural hand synergies for tool use. J Neuroscience 18.23: pp.10105-10115, 1998.

[15] Daffertshofer A, Lamoth CJ, Meijer OG, Peek BJ. PCA in studying coordination and variability: A tutorial. Clinical Biomechanics, 19.4: pp.415-428, 2004.

[16] Ranganathan R, Adewuyi A, Mussa-Ivaldi FA. Learning to be lazy: Exploiting redundancy in a novel task to minimize movement-related effort. J Neuroscience. 33.7: pp.2754-2760, 2013.

[17] Santello M, Baud-Bovy G, Jorntell H. Neural bases of hand synergies. Frontiers in Computational Neuroscience 7: pp.23, 2013.

[18] Ranganathan R, Wieser J, Mosier, KM, Mussa-Ivaldi FA, Scheidt RA. Learning redundant motor tasks with and without overlapping dimensions: Facilitation and interference effects. J Neurosci 34.24: pp.8289-8299, 2014.

[19] Fall, C. L., Turgeon, P., Campeau-Lecours, A., Maheu, V., Boukadoum, M., Roy, S., Massicotte, D., Gosselin, C., Gosselin, B. Intuitive wireless control of a robotic arm for people living with an upper body disability. Proc. Annual International Conference of the IEEE Engineering in Medicine and Biology Society, pp.4399-4402, 2015.

[20] Chapra, Steven C. Applied numerical methods. MATLAB for Engineers and Scientists. McGraw-Hill, 2012.